

# Excitonic Insulator State of the Extended Falicov–Kimball Model in the Cluster Dynamical Impurity Approximation

Kosuke Hamada<sup>1</sup>, Tatsuya Kaneko<sup>2</sup>, Shohei Miyakoshi<sup>1</sup>, and Yukinori Ohta<sup>1\*</sup>

<sup>1</sup>*Department of Physics, Chiba University, Chiba 263-8522, Japan*

<sup>2</sup>*Computational Condensed Matter Physics Laboratory, RIKEN, Wako, Saitama 351-0198, Japan*

We comparatively study the excitonic insulator state in the extended Falicov–Kimball model (EFKM, a spinless two-band model) on the two-dimensional square lattice using the variational cluster approximation (VCA) and the cluster dynamical impurity approximation (CDIA). In the latter, the particle-bath sites are included in the reference cluster to take into account the particle-number fluctuations in the correlation sites. We thus calculate the particle-number distribution, order parameter, ground-state phase diagram, anomalous Green’s function, and pair coherence length, thereby demonstrating the usefulness of the CDIA in the discussion of the excitonic condensation in the EFKM.

## 1. Introduction

The excitonic phases, often referred to as excitonic insulators (EIs), are the states where the valence and conduction bands are hybridized spontaneously by the inter-band Coulomb interaction, and have been predicted to occur near the semimetal-semiconductor phase boundary as the quantum condensation of electron-hole pairs (excitons).<sup>1–6</sup> In the semimetallic region, where the Coulomb interaction is largely screened by free carriers, the excitonic phase is described in analogy to the BCS theory of superconductivity, whereas in the semiconducting region, it is described as the Bose–Einstein condensation (BEC) of preformed excitons (or strongly bound electron-hole pairs). Thus, the BCS-BEC crossover is expected to occur by controlling the band gap from a negative value to a positive one.<sup>7–9</sup>

In recent years, the possible realization of spin-singlet excitonic condensation has been suggested for transition-metal chalcogenides such as  $1T$ -TiSe<sub>2</sub> and Ta<sub>2</sub>NiSe<sub>5</sub>.<sup>10–23</sup> The spin-triplet excitonic condensation has also been suggested to occur in the high-spin/low-spin crossover region of some cobalt oxide materials with the cubic perovskite structure.<sup>24–29</sup> Because these materials are among transition-metal chalcogenides and oxides, where the effects of electron correlations are strong, one must reconsider the excitonic phases from the standpoint of strongly correlated electron systems.<sup>30–32</sup> Thus, the lattice models such as Hubbard models, rather than the gas models, are appropriate for use. The spinless extended Falicov–Kimball model (EFKM) is the simplest lattice model for describing the excitonic phases, and has been used to discuss, for example, the BCS-BEC crossover of the excitonic condensation.<sup>33–41</sup> The multi-band Hubbard model, taking into account the spin de-

grees of freedom, has also been used to discuss, for example, the relative stability of the spin-singlet and spin-triplet excitonic phases.<sup>42–49</sup>

We have so far studied the excitonic phases of the EFKM and multiband Hubbard models using the variational cluster approximation (VCA) based on the exact diagonalization of small clusters.<sup>50, 51</sup> However, some difficulty arises in such a small-cluster approach, particularly when we calculate physical quantities as a function of the model parameters. For example, the number of electrons in the valence and conduction bands changes discontinuously as a function of energy-level splitting between the valence and conduction orbitals. This is because the number of electrons in the cluster is fixed, or the electron-number fluctuation in the cluster is prohibited, so that the finite-size effects appear even in the VCA,<sup>38, 44</sup> where the system of connecting the clusters is treated variationally in the thermodynamic limit.

In this paper, we therefore use the cluster dynamical impurity approximation (CDIA),<sup>52–54</sup> which is an extended version of the VCA, where the particle-bath sites are added to the reference clusters to take into account the electron-number fluctuations in the correlation sites. To the best of our knowledge, the roles of the bath sites in the multiorbital models have not been fully elucidated, so that the present study will provide a useful improvement of the VCA technique for two-orbital correlated electron models.

We will thus study the EI state of the EFKM defined on the two-dimensional square lattice, calculating the particle-number distribution, order parameter, ground-state phase diagram, anomalous Green’s function, and pair coherence length. We will show that the spurious discontinuities in the parameter dependence of some physical quantities, which are caused by the finite-size effect of the reference clusters and are inevitable in the VCA, are

\*ohta@faculty.chiba-u.jp

clearly suppressed in the CDIA. We thus demonstrate the usefulness of the CDIA in the discussion of the excitonic condensation of the EFKM.

This paper is organized as follows. In Sect. 2, we introduce the model and discuss the methods of calculation. In Sect. 3, we show the calculated physical quantities characterizing the excitonic phase of the EFKM and compare the results of the VCA with those of the CDIA to demonstrate the usefulness of the CDIA. A summary of the paper is given in Sect. 4.

## 2. Model and Method

### 2.1 Extended Falicov–Kimball Model

In this paper, we use the EFKM, which is the simplest lattice model to discuss the EI state.<sup>33–41</sup> Assuming a two-dimensional square lattice, we define the Hamiltonian of the EFKM as

$$\begin{aligned} \mathcal{H} = & -t_f \sum_{\langle i,j \rangle} f_i^\dagger f_j - t_c \sum_{\langle i,j \rangle} c_i^\dagger c_j + \frac{D}{2} \sum_i (n_{ic} - n_{if}) \\ & + U \sum_i n_{if} n_{ic} - \mu \sum_i (n_{if} + n_{ic}), \end{aligned} \quad (1)$$

where  $f_i^\dagger$  ( $c_i^\dagger$ ) and  $f_i$  ( $c_i$ ) denote the creation and annihilation operators of an electron on the  $f$  ( $c$ ) orbital at site  $i$ , respectively, and  $n_{if} = f_i^\dagger f_i$  ( $n_{ic} = c_i^\dagger c_i$ ).  $t_f$  ( $t_c$ ) is the transfer integral between the  $f$  ( $c$ ) orbital on the neighboring sites and  $D$  is the level splitting. Here, we assume  $D \geq 0$ , so that the  $f$  and  $c$  bands correspond to the valence and conduction bands, respectively.  $U$  ( $> 0$ ) is the interorbital Coulomb repulsion, leading to the excitonic instability in the system. The chemical potential  $\mu$  is determined to maintain the total particle density at half-filling:  $\langle n_f \rangle + \langle n_c \rangle = 1$ .

It is known that the EFKM at half-filling contains three phases: the staggered orbital ordered (SOO) phase, the EI phase, and the band insulator (BI) phase.<sup>33–35, 41</sup> At  $D = 0$ , where  $\langle n_f \rangle = \langle n_c \rangle = 0.5$ , the SOO phase appears, in which an electron occupies the  $c$  and  $f$  orbitals alternately. Comparison with the XXZ model obtained in the strong correlation limit of the EFKM indicates that the SOO phase becomes more stable when  $|t_c|/|t_f| \ll 1$ .<sup>34, 41</sup> On the other hand, when  $D \gg |t_f|, |t_c|$ , the BI phase appears, where  $\langle n_f \rangle = 1$  and  $\langle n_c \rangle = 0$ . Between these two phases, the EI phase appears, where the  $f$  and  $c$  orbitals hybridize spontaneously owing to the interaction  $U$ . With increasing  $U$  from the noninteracting semimetallic state, the EI state shows a smooth crossover from the weak-coupling BCS state to the strong-coupling BEC state.<sup>36–39</sup> Thus, the EFKM is used to discuss the BCS-BEC crossover of the excitonic condensation.

Hereafter, we assume  $t_f = t_c = t$  and use  $t$  as the unit of energy. When  $t_f = t_c$ , the SOO and EI phases have the same energy at  $D = 0$ , but at  $D > 0$ , the degeneracy is lifted and the EI phase becomes the most stable one.<sup>34, 41</sup> Note that the conduction-band bottom is lo-

cated at  $\mathbf{k} = (0, 0)$ , giving rise to an electron pocket, while the valence-band top is located at  $\mathbf{k} = (\pi, \pi)$ , giving rise to a hole pocket. Thus, the EI state of the present model is characterized by the modulation vector  $\mathbf{Q} = (\pi, \pi)$ . Throughout the paper, we set  $\hbar = 1$  and lattice constant  $a = 1$ . We fix the chemical potential at  $\mu = U/2$  because of the particle-hole symmetry at  $t_c = t_f$ .

### 2.2 VCA and CDIA

To accomplish the calculations treating electronic correlations accurately in the thermodynamic limit, we employ the VCA and CDIA, which are quantum cluster methods based on the self-energy functional theory (SFT).<sup>50–53</sup> In the SFT, the grand potential  $\Omega$  of the original system is given by a functional of the self-energy. In the VCA and CDIA, we introduce disconnected finite-size clusters that are solved exactly as a reference system. By restricting the trial self-energy to that of the reference system  $\hat{\Sigma}'$ , we obtain the grand potential in the thermodynamic limit as

$$\begin{aligned} \Omega[\hat{\Sigma}'] = & \Omega' + \text{Trln}(\hat{G}_0^{-1} - \hat{\Sigma}')^{-1} - \text{Trln}(\hat{G}') \\ = & \Omega' - \text{Trln}(\hat{I} - \hat{V}\hat{G}'), \end{aligned} \quad (2)$$

where  $\Omega'$  and  $\hat{G}'$  [ $= (\hat{G}_0'^{-1} - \hat{\Sigma}')^{-1}$ ] are the exact grand potential and Green's function of the reference system, respectively, and  $\hat{G}_0$  ( $\hat{G}_0'$ ) is the noninteracting Green's function of the original (reference) system.  $\hat{I}$  is the unit matrix and  $\hat{V} = \hat{G}_0'^{-1} - \hat{G}_0^{-1}$  corresponds to the hopping parameter between the adjacent clusters. In this method, the short-range electron correlations within the cluster of the reference system are taken into account exactly. Details of the method can be found in Refs. 55 and 56.

In our calculations, when a Hamiltonian of a reference system is given as  $\mathcal{H}'$ , we solve the eigenvalue problem  $\mathcal{H}'|\psi_0\rangle = E_0|\psi_0\rangle$  of a finite-size ( $L_c$  sites) cluster to obtain the ground state, and thus, the trial Green's function is calculated by the Lanczos exact-diagonalization method. The EFKM is a two-orbital model, and using the basis  $(f_i^\dagger, c_i^\dagger)$ , the Green's function matrix  $\hat{G}'$  in Eq. (2) may be written as

$$\hat{G}'(\omega) = \begin{pmatrix} \hat{G}'_{ff}(\omega) & \hat{G}'_{fc}(\omega) \\ \hat{G}'_{cf}(\omega) & \hat{G}'_{cc}(\omega) \end{pmatrix}, \quad (3)$$

where  $\hat{G}'^{\alpha\beta}$  is an  $L_c \times L_c$  matrix, and each matrix element is defined as

$$\begin{aligned} G'_{ij}{}^{\alpha\beta}(\omega) = & \langle \psi_0 | \alpha_i \frac{1}{\omega - \mathcal{H}' + E_0} \beta_j^\dagger | \psi_0 \rangle \\ & + \langle \psi_0 | \beta_j^\dagger \frac{1}{\omega + \mathcal{H}' - E_0} \alpha_i | \psi_0 \rangle. \end{aligned} \quad (4)$$

The advantage of the VCA is that the spontaneous symmetry breaking can be treated within the framework of the theory.<sup>51</sup> In this paper, we consider the EI state

of the EFKM, so that the Hamiltonian of the variational Weiss field is given as<sup>38)</sup>

$$\begin{aligned}\mathcal{H}'_{\text{EI}} &= \Delta' \sum_{\mathbf{k}} c_{\mathbf{k}+\mathbf{Q}}^\dagger f_{\mathbf{k}} + \text{H.c.} \\ &= \Delta' \sum_i e^{i\mathbf{Q}\cdot\mathbf{r}_i} c_i^\dagger f_i + \text{H.c.},\end{aligned}\quad (5)$$

where  $\mathbf{Q} = (\pi, \pi)$  in our indirect gap system ( $t_f = t_c$ ). Thus, in our VCA calculations, the Hamiltonian of the reference system is given as  $\mathcal{H}' = \mathcal{H} + \mathcal{H}'_{\text{EI}}$  and the variational parameter  $\Delta'$  is optimized on the basis of the variational principle,  $\partial\Omega/\partial\Delta' = 0$ . The solution with  $\Delta' \neq 0$  corresponds to the EI state. We use the 4-site 8-orbital cluster (s4-2o) and 8-site 16-orbital cluster (s8-2o) shown in Fig. 1(a) as the reference systems, where 2o denotes 2 orbitals per site.

A problem with the VCA is that the effects of the particle-number fluctuations are not fully taken into account because the number of electrons in the cluster of the reference systems is fixed. In particular, in the EFKM, the numbers of electrons in the  $f$  and  $c$  orbitals,  $N_f$  and  $N_c$ , respectively, which satisfy  $N_f + N_c = L$ , change discontinuously as a function of  $D$  when we calculate the ground state using the reference system of the exactly solved finite-size clusters. Although this discontinuity is partially relaxed when we introduce the variational parameter of the EI that yields the hybridization between the  $f$  and  $c$  orbitals, the effects of using the finite-size clusters in the reference system inevitably affect the results of the VCA calculations. Thus, the VCA, although formulated for calculations in the thermodynamic limit, cannot avoid the finite-size effects of the reference clusters.

To solve this problem, we use the CDIA,<sup>54,57,58)</sup> which is an extended version of the VCA, where the particle-bath sites are added to the clusters to take into account the electron-number fluctuations in the correlation sites, and is intrinsically equivalent to the cluster dynamical mean-field theory with an exact-diagonalization solver.<sup>59)</sup> In the CDIA, we introduce the hybridization parameter between the bath and correlation sites. We use the 2-site 4-orbital correlation cluster with 4 bath sites (s2-2o-2b) and 4-site 8-orbital correlation cluster with 8 bath sites (s4-2o-2b) as the reference systems, where 2o denotes 2 orbitals per site and 2b denotes 2 bath sites per correlation site, as shown in Fig. 1(a). In these reference systems, the variational Hamiltonian for the hybridization between the bath and correlation sites is given as  $\mathcal{H}'_{\text{hyb}} = V \sum_i (a_{if}^\dagger f_i + a_{ic}^\dagger c_i + \text{H.c.})$ , where  $a_{if}^\dagger$  ( $a_{ic}^\dagger$ ) is the creation operator of an electron at bath site  $i$  for the  $f$  ( $c$ ) orbital. The hybridization parameter  $V$  is optimized on the basis of SFT.<sup>54)</sup> In the CDIA, we must introduce the Weiss field for the EI in the bath sites, as well as in the correlation sites.<sup>59)</sup> The Weiss field in the present case is given by  $\mathcal{H}'_{\text{EI,b}} = -\Delta' \sum_i e^{i\mathbf{Q}\cdot\mathbf{r}_i} a_{ic}^\dagger a_{if} + \text{H.c.}$ , which en-

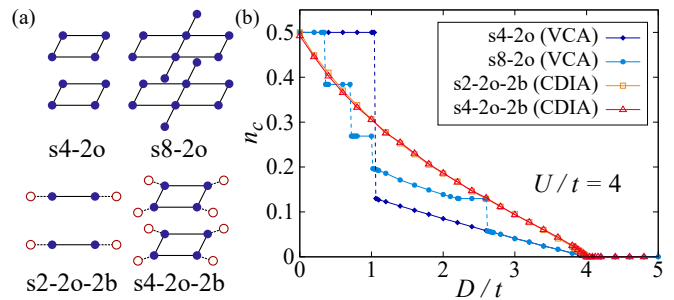


**Fig. 1.** (Color online) (a) Schematic representations of the reference clusters used in this paper. The 4-site 8-orbital (s4-2o), 8-site 16-orbital (s8-2o), 2-site 4-orbital 4-bath (s2-2o-2b), and 4-site 8-orbital 8-bath (s4-2o-2b) clusters are illustrated. (b) Calculated number of particles  $n_c$  as a function of  $D$  at  $U/t = 4$  obtained by the VCA and CDIA, where the normal phase without the EI order is assumed.

ables us to obtain physically meaningful solutions. Thus, in our CDIA calculations, the Hamiltonian of the reference system is given by  $\mathcal{H}' = \mathcal{H} + \mathcal{H}'_{\text{hyb}} + \mathcal{H}'_{\text{EI}} + \mathcal{H}'_{\text{EI,b}}$ , whereby we optimize the parameters  $V$  and  $\Delta'$  by applying the variational principle.

### 3. Results of Calculations

First, let us discuss the number of particles in the normal state ( $\Delta' = 0$ ) obtained using the VCA and CDIA. The average number of particles on the  $\alpha$  ( $=f, c$ ) orbital is given as

$$n_\alpha = \frac{1}{L} \sum_i \langle \alpha_i^\dagger \alpha_i \rangle = \frac{1}{N_c L_c} \oint_C \frac{dz}{2\pi i} \sum_{\mathbf{K}} \sum_{l=1}^{L_c} \mathcal{G}_{ll}^{\alpha\alpha}(\mathbf{K}, z), \quad (6)$$

where  $\hat{\mathcal{G}}^{\alpha\alpha}(\mathbf{K}, z)$  is the diagonal block (of size  $L_c \times L_c$ ) of the full matrix  $\hat{\mathcal{G}}(\mathbf{K}, z) = [\hat{G}'^{-1}(z) - \hat{V}(\mathbf{K})]^{-1}$  (of size  $2L_c \times 2L_c$ ). The  $\mathbf{K}$ -summation is performed in the reduced Brillouin zone of the superlattice,  $N_c$  is the number of clusters, and the contour  $C$  of the frequency integral encloses the negative real axis. In Fig. 1(b), we show the calculated results for the number of particles in the conduction band  $n_c$  as a function of  $D$ . We find that, in both the VCA and CDIA, the value of  $n_c$  decreases from 0.5 at  $D = 0$  to 0 at  $D \simeq 4$ , resulting in the BI at  $D \gtrsim 4$ . We then find that, in the VCA, the value of  $n_c$  changes discontinuously as a function of  $D$ , reflecting the discontinuous change in the number of particles obtained by the small-cluster diagonalization. However, in the CDIA, where the bath sites are introduced and the particle-number fluctuations are allowed, we find that the value of  $n_c$ , optimized by the variational calculation, decreases smoothly as a function of  $D$ , as is expected in the thermodynamic limit. We also find that the results for  $n_c$  depend little on the choice of the reference clusters s2-2o-2b and s4-2o-2b. The CDIA thus works very well for the present model.

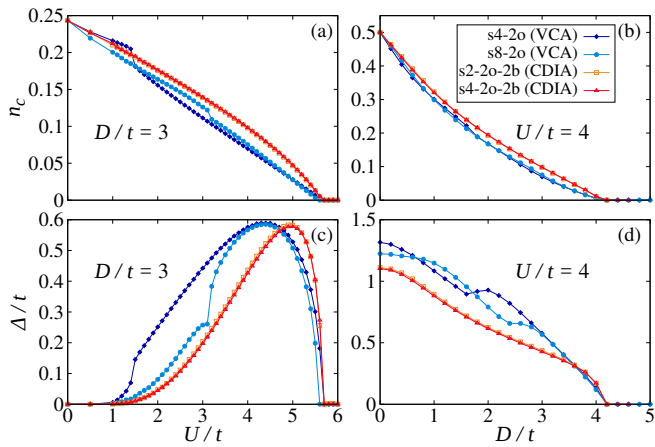


**Fig. 2.** (Color online) Calculated results for the particle number  $n_c$  and the order parameter  $\Delta$  in the EI state. Results of the VCA and CDIA are shown for comparison.  $U$  dependences are shown at  $D/t = 3$  in (a) and (c) and  $D$  dependences are shown at  $U/t = 4$  in (b) and (d).

Next, let us discuss the number of particles and the order parameter in the EI state ( $\Delta'_{\text{opt}} \neq 0$ ). The order parameter of the EI state is defined as

$$\begin{aligned} \Delta &= \frac{U}{L} \sum_{\mathbf{k}} \langle c_{\mathbf{k}+\mathbf{Q}}^\dagger f_{\mathbf{k}} \rangle = \frac{U}{L} \sum_i \langle c_i^\dagger f_i \rangle e^{i\mathbf{Q} \cdot \mathbf{r}_i} \\ &= \frac{U}{N_c L_c} \oint_C \frac{dz}{2\pi i} \sum_{\mathbf{K}} \sum_{l=1}^{L_c} \mathcal{G}_{ll}^{cf}(\mathbf{K}, z) e^{i\mathbf{Q} \cdot \mathbf{r}_l}, \quad (7) \end{aligned}$$

where  $\hat{\mathcal{G}}^{cf}(\mathbf{K}, z)$  is the off-diagonal block (of size  $L_c \times L_c$ ) of the full matrix  $\hat{\mathcal{G}}(\mathbf{K}, z)$ .

The number of particles  $n_c$  and the order parameter  $\Delta$  calculated by the VCA and CDIA are shown in the Fig. 2. Here, we first refer to some general aspects of the EI phase of the EFKM. We note in Fig. 2(a) that with increasing  $U$ , the effective energy-level difference increases owing to the Hartree shift, resulting in the BI phase at a large  $U$ . We also note in Fig. 2(c) that the order parameter increases with increasing  $U$ , reaches a peak at a certain  $U$  value, and then decreases rapidly as the system approaches the BI phase. This is a manifestation of the crossover between the BCS-like weak-coupling EI phase at small  $U$  and the BEC-like strong-coupling EI phase at large  $U$ .<sup>36–39</sup> We, moreover, note in Fig. 2(d) that the order parameter increases with decreasing  $D$  because the hole Fermi surface of the valence band and electron Fermi surface of the conduction band, which contribute to the formation of the EI phase, both become large with decreasing  $D$ . This is particularly the case when the Fermi surface nesting at the wave number  $\mathbf{Q}$  is perfect and the screening of the Coulomb interaction is absent, as in the present model. Imperfect Fermi surface nesting would change the present result considerably.

Now, let us compare the results of the VCA with those

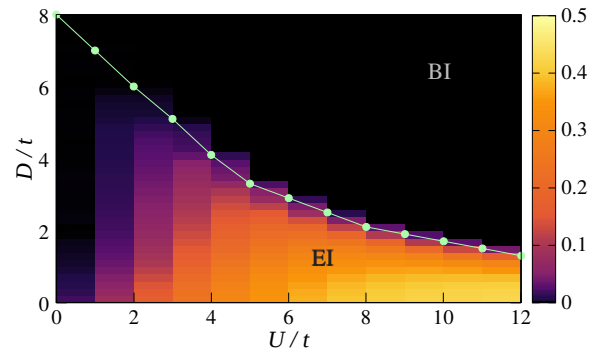


**Fig. 3.** (Color online) Calculated ground-state phase diagram of the EFKM in the CDIA. The order parameter  $\Phi = \Delta/U$  is indicated by color. The reference cluster s4-2o-2b was used.

of the CDIA. We first find in Figs. 2(a) and 2(b) that the discontinuous changes in  $n_c$  calculated in the VCA are weaker than those obtained for the normal state discussed above [see Fig. 1(b)]. This is because the nonvanishing variational parameter of the EI state, which corresponds to the band hybridization, allows the particle-number fluctuations between the  $f$  and  $c$  orbitals. However, we still find the discontinuities in  $n_c$  calculated in the VCA [see Fig. 2(a)], which are due to the finite-size effect of the reference cluster. The discontinuities are more serious in the calculated order parameter in the VCA, as shown in Fig. 2(c). The order parameter changes rather smoothly in the boundary region near the BI phase, where the band overlap is small, but in the region where the band overlap is large and the discontinuities in  $n_c$  are strong, the finite-size effect appearing in the order parameter becomes serious. In the CDIA, on the other hand, we find that the finite-size effects in the VCA are suppressed completely owing to the particle-number optimization by the bath sites, so that, using the CDIA, we can calculate the order parameter and  $n_c$  that change smoothly in a wide parameter space. Using the CDIA, we can thus calculate the order parameter in the EI state by suppressing the finite-size effects clearly. The ground-state phase diagram and order parameter  $\Phi = \Delta/U$  in the CDIA are then calculated and the results are shown in the  $U$ - $D$  plane in Fig. 3. We find that the transition point  $D_c$  between EI and BI phases decreases with increasing  $U$  and that the order parameter becomes large in the large- $U$  region below  $D_c$ .

Finally, to discuss the BCS-BEC crossover of the EI state in the EFKM, we calculate the particle momentum distribution function  $n_{\alpha}(\mathbf{k})$  and excitonic anomalous momentum distribution function  $F(\mathbf{k})$ <sup>38,44</sup> using Green's function in the cluster perturbation theory (CPT),<sup>60</sup> as given by

$$\hat{\mathcal{G}}_{\text{CPT}}(\mathbf{k}, \mathbf{k}', \omega) = \frac{1}{L_c} \sum_{i,j} \hat{\mathcal{G}}_{ij}(\mathbf{k}, \omega) e^{-i\mathbf{k} \cdot \mathbf{r}_i + i\mathbf{k}' \cdot \mathbf{r}_j}, \quad (8)$$

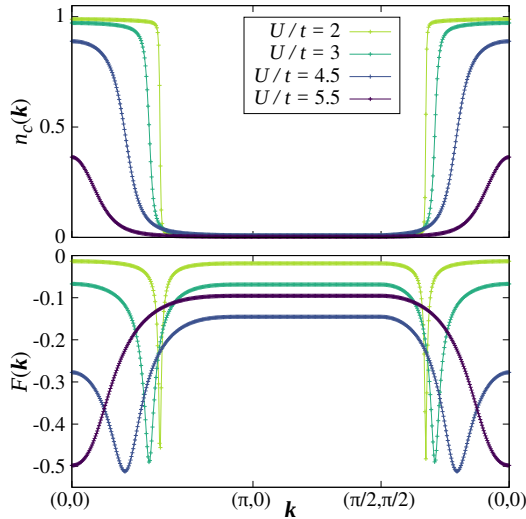


**Fig. 4.** (Color online) Calculated results for the electron momentum distribution function  $n_c(\mathbf{k})$  and anomalous momentum distribution function  $F(\mathbf{k})$  in the CDIA. The reference cluster s4-2o-2b was used and  $D/t = 3$  was assumed.

where  $\hat{\mathcal{G}}_{\text{CPT}}$  is a  $2 \times 2$  matrix. From this Green's function, the particle and anomalous momentum distribution functions are calculated as

$$n_\alpha(\mathbf{k}) = \oint_C \frac{dz}{2\pi i} \mathcal{G}_{\text{CPT}}^{\alpha\alpha}(\mathbf{k}, \mathbf{k}, z) \quad (9)$$

$$F(\mathbf{k}) = \oint_C \frac{dz}{2\pi i} \mathcal{G}_{\text{CPT}}^{cf}(\mathbf{k}, \mathbf{k} + \mathbf{Q}, z), \quad (10)$$

respectively. Using  $F(\mathbf{k})$ , we may also evaluate the pair coherence length  $\xi$ , the spatial size of the electron-hole pair, as<sup>38, 61, 62)</sup>

$$\xi^2 = \frac{\sum_{\mathbf{k}} |\nabla_{\mathbf{k}} F(\mathbf{k})|^2}{\sum_{\mathbf{k}} |F(\mathbf{k})|^2}. \quad (11)$$

The calculated results for the momentum distribution functions  $n_c(\mathbf{k})$  and  $F(\mathbf{k})$  are shown in Fig. 4, and those of the pair coherence length  $\xi$  are shown in Fig. 5. We find in Fig. 4 that for small  $U$ ,  $n_c(\mathbf{k})$  changes rapidly at the Fermi momentum  $\mathbf{k}_F$  defined by  $n_c(\mathbf{k}_F) = 0.5$ , but for large  $U$  near the BI phase,  $n_c(\mathbf{k})$  becomes small and broad in momentum space. We also find in Fig. 4 that  $F(\mathbf{k})$  shows a sharp peak at  $\mathbf{k}_F$  for small  $U$ , which broadens with increasing  $U$ . The sharp (broad) peak in  $F(\mathbf{k})$  indicates that the size of the electron-hole pair is large (small) in real space.<sup>38)</sup> This is evident in the calculated pair coherence length  $\xi$  shown in Fig. 5; i.e.,  $\xi$  is much larger (smaller) than the lattice constant for small (large)  $U$ . Thus, the BCS-BEC crossover occurs between the weak-coupling small- $U$  region and the strong-coupling large- $U$  region. Also noted in Fig. 5 is that  $\xi$  shows a discontinuous or kinklike structure in the VCA, which is clearly suppressed in the CDIA, similarly to the results

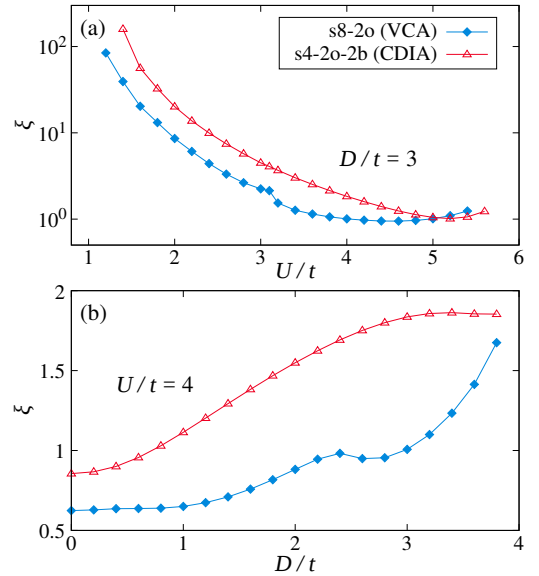


**Fig. 5.** (Color online) Pair coherence length  $\xi$  (in units of the lattice constant) calculated in the VCA and CDIA. (a)  $U$  dependence at  $D/t = 3$  and (b)  $D$  dependence at  $U/t = 4$  are shown.

for the particle number and order parameter shown in Fig. 2. These results thus demonstrate the usefulness of the CDIA in discussing the excitonic condensation in the EFKM.

#### 4. Summary

We studied the EI state of the EFKM defined on the two-dimensional square lattice, and calculated the particle-number distribution, order parameter, ground-state phase diagram, anomalous Green's function, and pair coherence length. We used the VCA and CDIA comparatively. We showed that the spurious discontinuities appearing in the parameter dependence of some physical quantities in the VCA are clearly suppressed in the CDIA, thus demonstrating that the addition of the particle-bath sites to take into account the electron-number fluctuations in the correlation sites provides an essential improvement of the VCA technique when we discuss the excitonic condensation of the EFKM.

We hope that the present study on the roles of the bath sites will offer useful improvements of the quantum cluster methods, such as the VCA, when they are applied to the multiorbital models.

We thank K. Seki and K. Sugimoto for enlightening discussions. This work was supported in part by a Grant-in-Aid for Scientific Research (No. 26400349) from JSPS of Japan. T. K. and S. M. acknowledge support from the JSPS Research Fellowship for Young Scientists.

1) L. V. Keldysh and Y. V. Kopeav, Sov. Phys. Solid State **6**,

- 2219 (1965).
- 2) J. Des Cloizeaux, *J. Phys. Chem. Solids* **26**, 259 (1965).
  - 3) D. Jérôme, T. M. Rice, and W. Kohn, *Phys. Rev.* **158**, 462 (1967).
  - 4) W. Kohn, *Phys. Rev. Lett.* **19**, 439 (1967).
  - 5) B. I. Halperin and T. M. Rice, *Rev. Mod. Phys.* **40**, 755 (1968).
  - 6) B. I. Halperin and T. M. Rice, in *Solid State Physics* (Academic, New York, 1968) Vol. 21, p. 115.
  - 7) A. N. Kozolov and L. A. Maksimov, *Sov. Phys. JETP* **21**, 790 (1965).
  - 8) P. Nozières and S. Schmitt-Rink, *J. Low Temp. Phys.* **59**, 195 (1985).
  - 9) F. X. Bronold and H. Fehske, *Phys. Rev. B* **74**, 165107 (2006).
  - 10) H. Cercellier, C. Monney, F. Clerc, C. Battaglia, L. Despont, M. G. Garnier, H. Beck, P. Aebi, L. Patthey, H. Berger, and L. Forró, *Phys. Rev. Lett.* **99**, 146403 (2007).
  - 11) C. Monney, H. Cercellier, F. Clerc, C. Battaglia, E. F. Schwier, C. Didiot, M. G. Garnier, H. Beck, P. Aebi, H. Berger, L. Forró, and L. Patthey, *Phys. Rev. B* **79**, 045116 (2009).
  - 12) J. van Wezel, P. Nahai-Williamson, and S. S. Saxena, *Phys. Rev. B* **81**, 165109 (2010).
  - 13) B. Zenker, H. Fehske, H. Beck, C. Monney, and A. R. Bishop, *Phys. Rev. B* **88**, 075138 (2013).
  - 14) G. Monney, C. Monney, B. Hildebrand, P. Aebi, and H. Beck, *Phys. Rev. Lett.* **114**, 086402 (2015).
  - 15) H. Watanabe, K. Seki, and S. Yunoki, *Phys. Rev. B* **91**, 205135 (2015).
  - 16) Y. Wakisaka, T. Sudayama, K. Takubo, T. Mizokawa, M. Arita, H. Namatame, M. Taniguchi, N. Katayama, M. Nohara, and H. Takagi, *Phys. Rev. Lett.* **103**, 026402 (2009).
  - 17) T. Kaneko, T. Toriyama, T. Konishi, and Y. Ohta, *Phys. Rev. B* **87**, 035121 (2013); **87**, 199902(E) (2013).
  - 18) K. Seki, Y. Wakisaka, T. Kaneko, T. Toriyama, T. Konishi, T. Sudayama, N. L. Saini, M. Arita, H. Namatame, M. Taniguchi, N. Katayama, M. Nohara, H. Takagi, T. Mizokawa, and Y. Ohta, *Phys. Rev. B* **90**, 155116 (2014).
  - 19) K. Sugimoto, T. Kaneko, and Y. Ohta, *Phys. Rev. B* **93**, 041105(R) (2016).
  - 20) K. Sugimoto and Y. Ohta, *Phys. Rev. B* **94**, 085111 (2016).
  - 21) T. Yamada, K. Domon, and Y. Ōno, *J. Phys. Soc. Jpn.* **85**, 053703 (2016).
  - 22) S. Mor, M. Herzog, D. Golež, P. Werner, M. Eckstein, N. Katayama, M. Nohara, H. Takagi, T. Mizokawa, C. Monney, and J. Stähler, arXiv:1608.05586.
  - 23) Y. F. Lu, H. Kono, T. I. Larkin, A. W. Rost, T. Takayama, A. V. Boris, B. Keimer, and H. Takagi, *Nat. Commun.* **8**, 14408 (2017).
  - 24) J. Kuneš and P. Augustinský, *Phys. Rev. B* **90**, 235112 (2014).
  - 25) A. Ikeda, T. Nomura, Y. H. Matsuda, A. Matsuo, K. Kindo, and K. Sato, *Phys. Rev. B* **93**, 220401 (2016).
  - 26) J. Nasu, T. Watanabe, M. Naka, and S. Ishihara, *Phys. Rev. B* **93**, 205136 (2016).
  - 27) A. Sotnikov and J. Kuneš, *Sci. Rep.* **6**, 30510 (2016).
  - 28) T. Tatsuno, E. Mizoguchi, J. Nasu, M. Naka, and S. Ishihara, *J. Phys. Soc. Jpn.* **85**, 083706 (2016).
  - 29) T. Yamaguchi, K. Sugimoto, and Y. Ohta, *J. Phys. Soc. Jpn.* **86**, 043701 (2017).
  - 30) J. Kuneš, *J. Phys.: Condens. Matter* **27**, 333201 (2015).
  - 31) T. Kaneko and Y. Ohta, *Phys. Rev. B* **94**, 125127 (2016).
  - 32) Y. Ohta, T. Kaneko, and K. Sugimoto, *Kotai Butsuri* **52**, 119 (2017) [in Japanese].
  - 33) C. D. Batista, *Phys. Rev. Lett.* **89**, 166403 (2002).
  - 34) C. D. Batista, J. E. Gubernatis, J. Bonča, and H. Q. Lin, *Phys. Rev. Lett.* **92**, 187601 (2004).
  - 35) P. Farkašovský, *Phys. Rev. B* **77**, 155130 (2008).
  - 36) D. Ihle, M. Pfaffertott, E. Burovski, F. X. Bronold, and H. Fehske, *Phys. Rev. B* **78**, 193103 (2008).
  - 37) V.-N. Phan, K. W. Becker, and H. Fehske, *Phys. Rev. B* **81**, 205117 (2010).
  - 38) K. Seki, R. Eder, and Y. Ohta, *Phys. Rev. B* **84**, 245106 (2011).
  - 39) B. Zenker, D. Ihle, F. X. Bronold, and H. Fehske, *Phys. Rev. B* **85**, 121102 (2012).
  - 40) T. Kaneko, S. Ejima, H. Fehske, and Y. Ohta, *Phys. Rev. B* **88**, 035312 (2013).
  - 41) S. Ejima, T. Kaneko, Y. Ohta, and H. Fehske, *Phys. Rev. Lett.* **112**, 026401 (2014).
  - 42) P. M. R. Brydon and C. Timm, *Phys. Rev. B* **80**, 174401 (2009).
  - 43) B. Zocher, C. Timm, and P. M. R. Brydon, *Phys. Rev. B* **84**, 144425 (2011).
  - 44) T. Kaneko, K. Seki, and Y. Ohta, *Phys. Rev. B* **85**, 165135 (2012).
  - 45) J. Kuneš and P. Augustinský, *Phys. Rev. B* **89**, 115134 (2014).
  - 46) J. Kuneš, *Phys. Rev. B* **90**, 235140 (2014).
  - 47) T. Kaneko and Y. Ohta, *Phys. Rev. B* **90**, 245144 (2014).
  - 48) T. Kaneko, B. Zenker, H. Fehske, and Y. Ohta, *Phys. Rev. B* **92**, 115106 (2015).
  - 49) J. Kuneš and D. Geffroy, *Phys. Rev. Lett.* **116**, 256403 (2016).
  - 50) M. Potthoff, M. Aichhorn, and C. Dahnen, *Phys. Rev. Lett.* **91**, 206402 (2003).
  - 51) C. Dahnen, M. Aichhorn, W. Hanke, E. Arrigoni, and M. Potthoff, *Phys. Rev. B* **70**, 245110 (2004).
  - 52) M. Potthoff, *Eur. Phys. J. B* **32**, 429 (2003).
  - 53) M. Potthoff, *Eur. Phys. J. B* **36**, 335 (2003).
  - 54) M. Balzer, B. Kyung, D. Sénéchal, A.-M. S. Tremblay, and M. Potthoff, *Europhys. Lett.* **85**, 17002 (2009).
  - 55) M. Potthoff, in *Strongly Correlated Systems — Theoretical Methods*, Vol. 171 of *Springer Series in Solid-State Sciences* (Springer-Verlag, Berlin Heidelberg, 2012) Chap. 10, p. 303.
  - 56) D. Sénéchal, arXiv:0806.2690.
  - 57) S. R. Hassan and D. Sénéchal, *Phys. Rev. Lett.* **110**, 096402 (2013).
  - 58) M. Ebato, T. Kaneko, and Y. Ohta, *J. Phys. Soc. Jpn.* **84**, 044714 (2015).
  - 59) D. Sénéchal, in *Strongly Correlated Systems — Theoretical Methods*, Vol. 171 of *Springer Series in Solid-State Sciences* (Springer-Verlag, Berlin Heidelberg, 2012) Chap. 11, p. 341.
  - 60) D. Sénéchal, D. Perez, and M. Pioro-Ladrière, *Phys. Rev. Lett.* **84**, 522 (2000).
  - 61) Y. Ohta, A. Nakauchi, R. Eder, K. Tsutsui, and S. Maekawa, *Phys. Rev. B* **52**, 15617 (1995).
  - 62) T. Kaneko and Y. Ohta, *J. Phys. Soc. Jpn.* **83**, 024711 (2014).